Forming mechanism of refined granular crystalline of $Cu_{70}Ni_{30}$ alloy by undercooled solidification*

GUO Xuefeng (郭学锋)[1,2], LIU Feng (刘 峰)[1], YANG Gencang (杨根仓)[1] and XING Jiandong (邢建东)[3]

(1. State Key Laboratory of Solidification Processing, Northwestern Polytechnical University, Xi'an 710072, China;
2. College of Materials Science and Engineering, Xi'an University of Technology, Xi'an 710048, China;
3. School of Mechanical Engineering, Xi'an Jiaotong University, Xi'an 710049, China)

Received February 14, 2000; revised March 13, 2000

Abstract Both glass fluxing and cyclic superheating techniques were adopted to effectively undercool the $Cu_{70}Ni_{30}$ alloy in vacuum. Within the undercooling range of 21 K to 270 K, the microstructure evolution of the alloy was investigated. When the melt was undercooled to $\Delta T > \Delta T_3'$ (210 K), the grain refinement took place abruptly. Based on the observation of the solidified microstructure, the microchemical-analysis and the calculated results with BCT model, it is found that the secondary grain refinement mechanism consists of two stages. The dendrite is, firstly, broken into fragments owing to the stress caused by uneven shrinking during rapid solidification, then the fragments, under the driving force of surface and strain energies, merge through the migration of boundaries, i. e. recrystallization, thus leading to the formation of secondary granular-crystalline.

Keywords: undercooling, $Cu_{70}Ni_{30}$ alloy, dendrite breaking, recrystallization.

The grain refinement phenomenon[1,2] in undercooled pure metals and single phase alloys was first found in pure nickel by Walker[3], in which the grain size abruptly decreased by 2 orders of magnitude when the undercooling prior to nucleation exceeded a critical value ΔT^*. Then the phenomenon of grain size reduction was also observed in Cu-Ni[4], Fe-Ni[1] and Cu-O[2] alloy systems, which indicated that the grain refinement was a rather common process in the microstructural evolution of the undercooled single phase alloys[5]. Several mechanisms have been suggested to explain this phenomenon. For example, the copious homogeneous nucleation[6,7], the remelting of primary dendrite[1,8], the primary dendrite recrystallization during recalescence and post-recalescence stages[2], the critical growth velocity[4] and the broken-up model[5] were proposed. Recently two kinds of granularization in the lower and higher undercooling ranges were observed in the solidified microstructure of the undercooled single-phase alloy melt[9]. The break-up of dendritic remelting had been proposed to explain the grain refinement in the lower undercooling range[1, 10]. Though much attention had been paid to the secondary granularization in the high undercooling range, the refinement mechanism was still an open question[9]. In this paper, the secondary granular-crystalline formed in the solidification process of undercooled $Cu_{70}Ni_{30}$ melt is investigated. Based on theoretical thermal dynamic calcula-

* Projects supported by the National Natural Science Foundation of China (Grant No. 59871041) and Natural Science Foundation of Shaanxi Province (Grant No. 98C13).

tion, microchemical analysis and the observation of the solidified microstructure, it is found that the formation of the secondary granular-crystalline is attributed neither to the dendrite remelting, nor to the recrystallization alone. The grain refinement mechanism consists of two consecutive stages. The dendrite is, firstly, broken into fragments owing to the stress caused by uneven shrinking during rapid solidification. And then the fragments, under the driving force of surface and strain energies, merge through boundary migrations, i. e. recrystallization, leading to the formation of secondary granular-crystalline.

1 Experimental

The undercooling experiments were performed in a high-frequency induction heater. High purity nickel and copper (purer than 99.9 percent) were melted *in situ* in a quartz crucible to obtain an alloy with a composition of $Cu_{70}Ni_{30}$. To achieve large undercooling, the glass (with granularity of 2—4 mm) and alloy particles for purification were previously set in a crucible[11]. During the undercooling experiment, the melting chamber was evacuated to 1.33×10^{-4} Pa and the alloy was heated to 1 173—1 273 K and covered with softening purification glass, then to 1 637 K the alloy was degassed for 2 min. After the melt was superheated to 1 823—1 837 K and held for 2 min, the melt was cooled down naturally. When the above heating and cooling process was performed twice, various solidification structures could be obtained by triggering the melt surface with a nickel needle under different undercooling condition.

The cooling curves of the melts were measured by an infrared pyrometer with a response time of 1 ms, and relative accuracy of ± 5 K. The absolute temperature of the pyrometer was calibrated with a standard PtRh30-PtRh6 thermocouple.

For microstructural analysis, the undercooled samples were sectioned and polished using standard microscopic techniques. The polished samples were then etched in a ferric nitride solution for observing grain boundaries and in ferric chloride solution for observing dendrite morphologies. A scanning electron microscope with a TN-5 400 EPMA energy-dispersive spectrometer was used to carry out the micro-composition analysis.

2 Results

When the $Cu_{70}Ni_{30}$ melts are solidified in the undercooling range of 22—270 K, there exist three kinds of microstructural transformations, resulting in four kinds of microstructure morphologies (as shown in fig. 1). When $\Delta T < \Delta T_2^*$ (120 K), the solidification morphology evolves with the increasing undercoolings into the first granular-crystalline (see fig.1(b)) from the highly branched dendrite (see fig.1(a)), as a result of dendrite break-up owing to remelting and subsequent recrystallization. In the undercooling range of $\Delta T_2^* < \Delta T < \Delta T_3^*$ (210 K), the undercooled dendrite is formed step by step from the first granular-crystalline owing to the restrained dendrite remelting[9] (see fig. 1(c)). When the undercooling exceeds ΔT_3^*, the second granularization occurs (figs.1(d) and (e)). Here the critical undercoolings of ΔT_2^* and ΔT_3^* were confirmed by the continuous observation of the microstructure evolution during solidification.

Figure 2 shows the solidified microstructure at $\Delta T = \Delta T_3^*$, in which the dendrite-like mi-

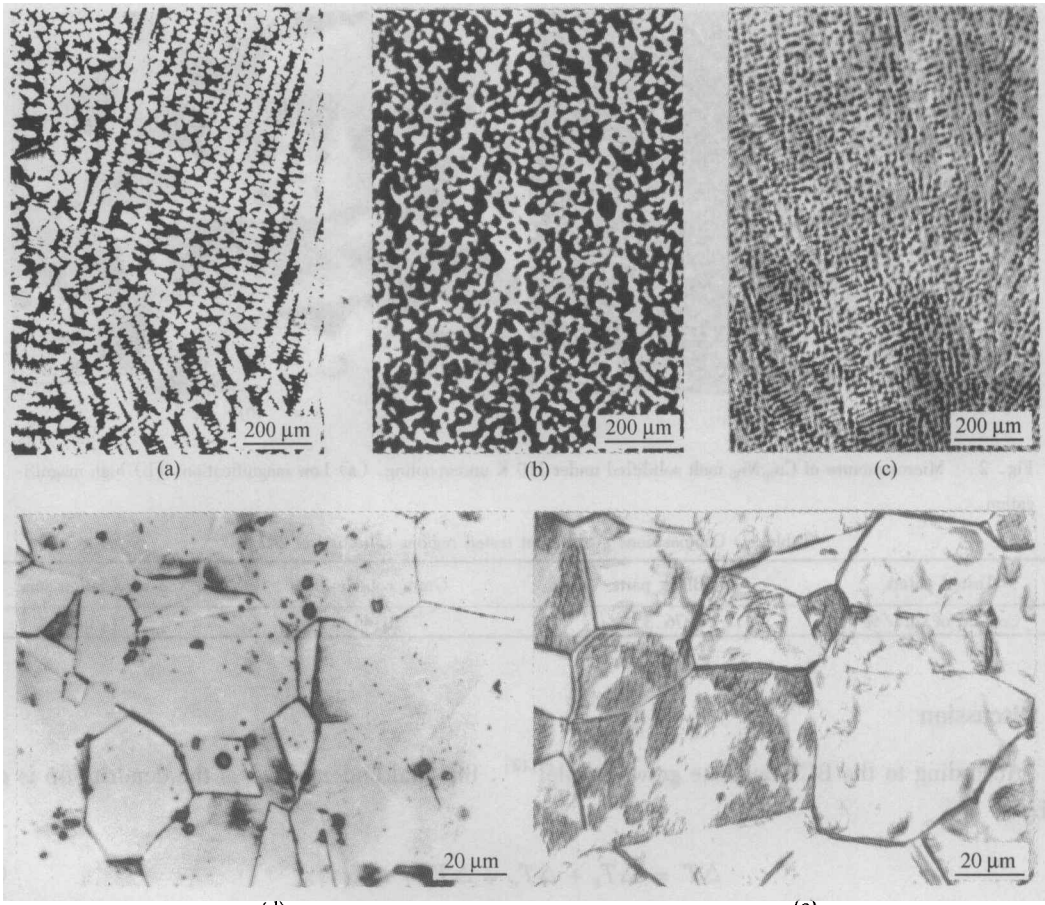

Fig. 1. Solidified microstructures of $Cu_{70}Ni_{30}$ under different undercoolings. (a) $\Delta T = 22$ K; (b) $\Delta T = 71$ K; (c) $\Delta T = 132$ K; (d) $\Delta T = 230$ K; (e) $\Delta T = 242$ K.

crostructure eradiates into the undercooled melt from the triggered site with weak directional characteristics. Comparing with the undercooled dendrite, the break-up degree of this microstructure is more serious, but not enough for the formation of dendritic units[1].

While observing the evolution of this microstructure, it is found that just as the transformation from the undercooled dendrite to the second granular-crystalline begins, the grain boundaries originating from the sharp angles of the dendritic microporosity are starting to cut into the dendritic arms (see fig.2(b)). From the solidified microstructure shown in figs. 1(d) and (e), a large amount of grain boundaries have cut across the dendritic arms, except a few of them cut through the so-called black parts (the segregation zone, the lastly solidified part), which are distributed homogeneously in the substrate microstructure. The result of EDS analysis shows that the composition near the grain boundaries is close to that of the non-segregation zones, however, obvious difference exists between the non-segregation zones and the black parts, as shown in table 1.

With the increase of undercooling, the solidified microstructure is close to that of the annealed hexagonal grains, with a great deal of annealed twins, as shown in figures 1 (d), and 1 (e).

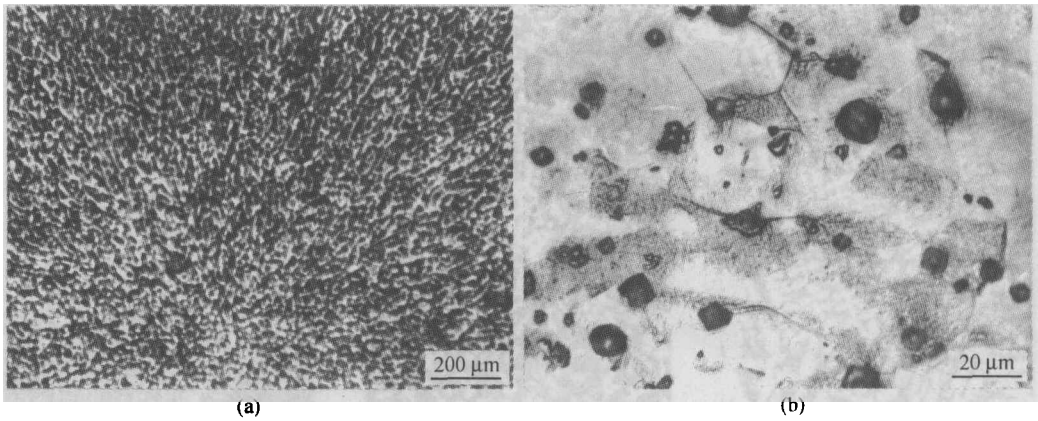

Fig. 2. Microstructure of $Cu_{70}Ni_{30}$ melt solidified under 210 K undercooling. (a) Low magnification, (b) high magnification.

Table 1 Compositions at different tested regions solidified at 242 K

Tested points	Black parts	Grain boundaries	Non-segregation zone
Content of Cu, / %	76.35	70.44	71.36

3 Discussion

According to the BCT dendrite growth model[12], the total undercooling at the dendrite tip is given by

$$\Delta T = \Delta T_t + \Delta T_c + \Delta T_r + \Delta T_k, \tag{1}$$

where the thermal undercooling ΔT_t is the difference between the temperature T_i at the dendrite tip and the temperature T_∞ of the undercooled liquid far ahead, and the sum $\Delta T_c + \Delta T_r + \Delta T_k$ is related to the difference between the equilibrium melting temperature T_L of the alloy and T_i, which is due to the constitutional undercooling ΔT_c, the Gibbs-Thomson effect (curved solid-liquid interface, ΔT_r) and the kinetic effects at the interface ΔT_k. ΔT_t is given by the steady-state solution of the corresponding diffusion equations,

$$\Delta T_t = \frac{\Delta H}{C_P} Iv(P_t), \tag{2}$$

where ΔH is the latent heat of fusion per unit volume, C_P the heat capacity of the liquid per unit volume, P_t the thermal Peclet number, and $Iv(P)$ the Ivantsov function. The constitutional undercooling ΔT_c is given by

$$\Delta T_c = m_L C_0 \left[1 - \frac{m'/m_L}{1 - (1 - k) Iv(P_c)} \right], \tag{3}$$

where C_0 is the alloy composition, P_c the solute Peclet number, m_L the equilibrium liquidus slop, k the effective solute distribution coefficient, and the effective liquidus slope m' is given by[12]

$$m' = m_L\left[1 + \frac{k_0 - k(1 - (\ln k)/k_0)}{1 - k_0}\right], \tag{4}$$

To take into account the solute trapping effect at high growth velocities, the partition coefficient k could be expressed in terms of velocity as suggested by Aziz[13]

$$k = \frac{k_0 + (a_0/D)V}{1 + (a_0/D)V}, \tag{5}$$

where k_0 is the equilibrium solute distribution coefficient and a_0 the interatomic distance.

The curvature undercooling is given by

$$\Delta T_r = \frac{2\Gamma}{r}, \tag{6}$$

where Γ is the Gibbs-Thomson parameter (equal to $\sigma/\Delta S$, in which σ is the interfacial energy and ΔS the entropy of fusion).

The kinetic undercooling is given by

$$\Delta T_k = \frac{V}{\mu}, \tag{7}$$

$$\mu = \frac{\Delta H V_0}{k_B T_L^2}. \tag{8}$$

where k_B is the Boltzmann constant and V_0 the sound transmission speed in the melt.

The solution of eq. (1) is obtained by applying the marginal stability criterion to the dendrite with the tip radius equal to the shortest stable wavelength. The dendrite tip radius is given by[14]

$$r = \frac{\sigma/(\Delta S\sigma^*)}{\frac{P_t \Delta H}{C_p}\xi_t + \frac{2m'P_C C_0(k-1)}{1-(1-k)Iv(P_c)}\xi_c}, \tag{9}$$

$$\xi_t = 1 - \frac{1}{\sqrt{1 + \frac{1}{\sigma^* P_t^2}}}, \qquad \xi_c = 1 + \frac{2k}{1 - 2k - \sqrt{1 + \frac{1}{\sigma^* P_c^2}}}, \tag{10}$$

and σ^* is the stability constant (equal to $\sigma^* = 1/4\pi^2$).

The solute (copper) concentration of the liquid (C_L^*) and solid (C_S^*) at the dendrite tip can be written as[4]

$$C_L^* = \frac{C_0}{1 - (1-k)Iv(P_c)}, \qquad C_S^* = \frac{kC_0}{1 - (1-k)Iv(P_c)}. \tag{11}$$

The solid fraction f_S during rapid solidification is given by

$$f_S = \frac{C_L^* - C_0}{C_L^*(1-k)}. \tag{12}$$

Assuming that recalescence process is adiabatic, the specific heat of solid and liquid are equal, the compositions of solid and liquid after recalescence are uniform[15], the solid fraction f_S^R, at the maximum recalescence temperature T_R, is given by

$$f_S^R = \frac{T_R - T_N}{\Delta H / C_p}. \tag{13}$$

where T_N is the nucleation temperature. The solute balance can be described as

$$f_S^R C_S^R + (1 - f_S^R) C_L^R = C_0, \tag{14}$$

where C_L^R and C_S^R are liquid and solid compositions at T_R. They are given as follows:

$$C_L^R = C_0 + \frac{T_R - T_L}{m_L}, \quad C_S^R = k_0 C_L^R. \tag{15}$$

The remelted solid fraction Δf_s after recalescence can be written as[15]

$$\Delta f_S = f_S - f_S^R. \tag{16}$$

According to the equilibrium phase diagram, the dendrite composition C_S^* and the corresponding equilibrium solidus in the rapid solidification process could be calculated. Therefore, the superheating ΔT_h in recalescence can be expressed as

$$\Delta T_h = T_R - T_S. \tag{17}$$

where T_S is the equilibrium solidus temperature.

During a rapid solidification, dendrite grows radially from the triggered site and a spherical liquid/solid mush-zone is formed. Thus the mush-zone-forming rate Q is given by

$$Q = \frac{4}{3}\pi[V]^3. \tag{18}$$

And the volume transformation rate Q_L from liquid to solid is given by

$$Q_L = Q \cdot f_S. \tag{19}$$

Suppose that the volume transformation rates of pure copper and nickel in melting process are ΔQ_{Cu} and ΔQ_{Ni}, then the volume transformation rate in the alloy melting process for regular solid solution will be

$$\Delta Q_m = x \cdot \Delta Q_{Cu} + (1 - x) \cdot \Delta Q_{Ni}, \tag{20}$$

where x is the mole fraction of copper in alloy.

Based on the conception of the volume transformation rate in alloy melting process

$$\Delta Q_m = \frac{Q_L - Q_S}{Q_S} \times 100\% , \tag{21}$$

the volume transformation rate of solidification, $(Q_L - Q_s)$, under different undercoolings is

$$(Q_L - Q_S) = \frac{4}{3}\pi \frac{C_L - C_0}{C_L(1-k)}\left[\frac{\Delta Q_m}{1+\Delta Q_m}\right] \cdot [V]^3. \tag{22}$$

The calculated results of the above quantities as a function of the bulk undercooling are shown in figs. 3—7 using eqs. (1)—(22). Fig. 3 presents the calculated curves for dendrite tip radius and undercooling contributions. Fig. 4 shows the liquid/solid compositions in the dendrite tip. Fig. 5 shows

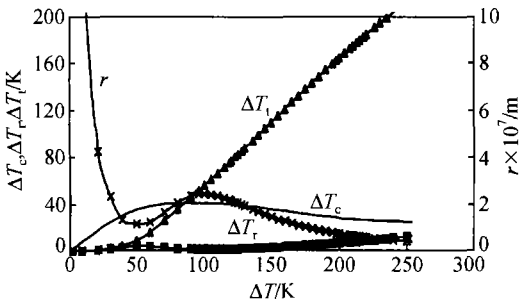

Fig. 3. Relationships of ΔT_c, ΔT_t, ΔT_r and r with bulk ΔT.

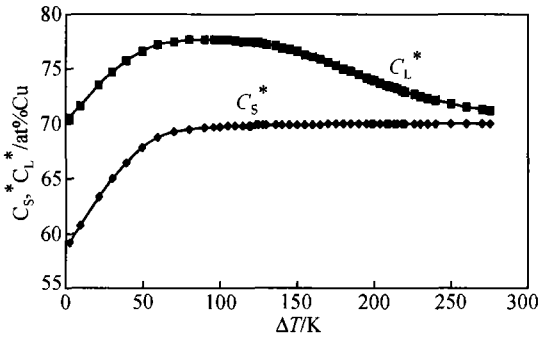

Fig. 4. Relationships of C_L^* and C_S^* with bulk ΔT.

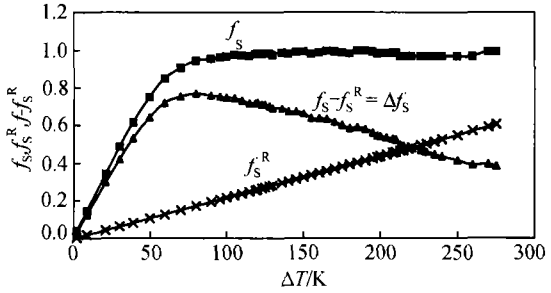

Fig. 5. Relationships of f_s, f_s^R and Δf_s with bulk ΔT.

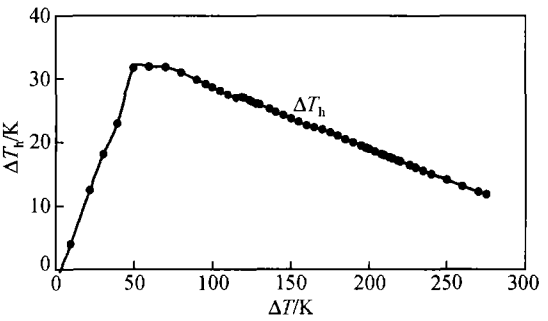

Fig. 6. Relationship of ΔT_h with bulk ΔT.

the solid fraction f_s in the process of rapid solidification, the post-recalescence solid fraction f_s^R and the remelted solid fraction Δf_s in the post-reca lescence process, respectively. Fig. 6 shows the recalescence superheating. The volume transformation rate during solidification is shown in fig. 7. The thermophysical parameters used for the calculation are given in table 2[16].

In the achieved undercooling range, both the constitutional undercooling and thermal undercooling play the decisive role in the solidification process.

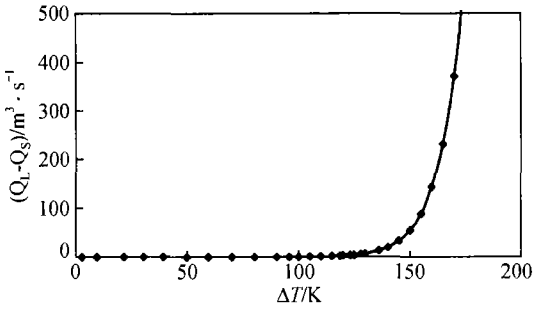

Fig. 7. Relationship of Q_L-Q_s with bulk ΔT.

When $\Delta T > 90$ K, as shown in fig. 3, the thermal undercooling contribution is higher than the constitutional one, which means there is a progressive transformation from the dendrite growth controlled by constitutional diffusion to that controlled by pure thermal diffusion. The higher the undercooling and the more the thermal undercooling contribution, the more the dissipation of latent heat in the tip of dendrite will be. Furthermore, because of the heat-absorption of the undercooled melt in recalescence, the recalescence superheating will decrease (see fig. 6) and the copper content in liquid/solid phase (see fig. 4) will also decrease, resulting in a highly supersaturated crystal. The result shows the decrease of dendrite remelting fraction during solidification (see fig. 5), and finally, the ripening of dendrite is restrained. So the fine dendrite structure which is defined as undercooled dendrite (see fig. 1(c)) is formed when $\Delta T > 120$ K. For the bulk undercooling beyond ΔT_3^*, although the dendrite radius formed in rapid solidification is less than 0.664×10^{-7}m (as shown in fig. 3), the recalescence superheating is less than 17.9 K (as shown in fig .6). Then, C_S^* is close to C_0, and the copper content in liquid C_L^* decreases (as shown in fig. 4). So the dendrite-remelting fraction $f_S - f_S^R$ decreases, and the solid fraction f_s^R is greater than 0.472 (as shown in fig. 5) in the post-recalescence. All the factors which are favorable for the remelting process of the dendrite are not better than the condition of $\Delta T < \Delta T_3^*$. Therefore, it can be inferred that the formation of the granular-crystalline is not likely attributed to the dendrite break-up owing to remelting. This result is also proved by the EDS analysis. Otherwise, the high-angled boundaries should appear at the lastly solidified zone by epitaxial growth of remelted fragments.

Table 2 Values of the material parameters of $Cu_{70}Ni_{30}$ alloy used in the calculations

Parameters	Values	Parameters	Values
ΔH/J·m^{-3}	2.062×10^9	ΔC_p/J·m^{-3}·K^{-1}	5.126×10^6
a/m^2·s^{-1}	3.0×10^{-6}	D/m^2·s^{-1}	6.0×10^{-9}
σ/J·m^{-2}	0.374	k_0	1.381
m/K·(at%)$^{-1}$	5.373	a_0/m	3.0×10^{-10}
V_0/m·s^{-1}	2000	T_L/K	1510
ΔQ_{Cu}/%	4.2	ΔQ_{Ni}/%	4.5

From eq. (22), it is known that $(Q_L-Q_S) \propto V^3$ and $V \propto \Delta T^b$, here b is a constant[17] independent of undercooling. Therefore, when the bulk undercooling exceeds a critical value, the volume transformation rate from liquid to solid can increase rapidly. Comparing the value of (Q_L-Q_S), which is 6.88×10^{-5}m^3/s at the undercooling of 39 K, with that of 9.95×10^3m^3/s at the undercooling of ΔT_3^*, it is really an increase of 8 orders of magnitude (as shown in fig. 7). During rapid solidification, the non-homogeneous contraction, which is found to cause a sharp increase of the internal stress and plastic energy in the solid phase, leads to the complete disintegration of dendrite and the formation of dendritic fragments as shown in fig. 2(a). Then, the dendrite disintegration will give rise to an increase in system surface energy, which, combined with the plastic energy, drives the dendritic

fragments to merge into final granular-crystalline through the crystal boundary migration at high temperature. The higher the undercooling, the faster the boundary migration and growth, and the more the twins in solidification structure will be. It is well known that any boundary migration at high temperature could be a recrystallization process. Thus the formation of the secondary granular-crystalline is due to the dendrite disintegration and the subsequent recrystallization.

4 Conclusions

(i) Within the achieved undercooling range, 22—270 K, three transformation stages occur in the microstructure evolution of single phase $Cu_{70}Ni_{30}$ alloy, and consequently, four kinds of morphologies appear, which are highly branched dendrites, primary granular crystalline, dendrites, and secondary granular crystalline.

(ii) The formation of the secondary granular-crystalline is due to the dendrite disintegration owing to the extremely high stress of the non-homogeneous contraction during solidification, and the migration of the boundary at high temperature.

References

1 Kattamis, T. Z., Flemings, M. C., Dendrite structure and grain size of undercooled melts, *Trans. Met. Soc. AIME*, 1966, 236: 1523.

2 Powell, G. L. F., Hogan, L. M., The influence of oxygen content on the grain size of undercooled silver, *Trans. Met. Soc. AIME*, 1969, 245: 407.

3 Walker, J. L., *Physical Chemistry of Process Metallurgy*: Part 2 (ed. Pierre, G. R. St.) New York: Interscience Publishers, 1964, 845.

4 Herlach, D. M., Non-equilibrium solidification of undercooled metallic melts, *Mater. Sci. Eng.*, 1994, R12: 177.

5 Schwarz, M., Karma, A., Eckler, K. et al., Physical mechanism of grain refinement in solidification of undercooled melts, *Phys. Rev. Lett.*, 1994, 73: 1380.

6 Horvay, G. J., The tension field created by a spherical nucleus freezing into its less dense undercooled melt, *Heat Mass Transfer*, 1965, 8: 195.

7 Glicksman, M. E., Dynamic effects arising from high-speed solidification, *Acta Metall.*, 1965, 13: 1231.

8 Jackson, K. A., Hunt, J. D., Uhlmann, D. R. et al., On the origin of the equiaxed zone in castings, *Trans. TMS-AIME*, 1966, 236: 149.

9 Gartner, F., Ramous, E., Herlach, D. M. et al., Texture analysis of the development of microstructure in Cu-30 at.% Ni alloy droplets solidified at selected undercoolings, *Acta Mater.*, 1997, 45: 51.

10 Cochrane, R. F., Herlach, D. M., Feuerbacher, B., Grain refinement in drop-tube-processed nickel-based alloys, *Mater. Sci. Eng.*, 1991, A133: 706.

11 Guo, X. F., Yang, G. C., Xing, J. D., The effect of glass composition on the undercooling stability of Cu-Ni alloy, *Foundry Technology* (in Chinese), 1999, 114(5): 47.

12 Boettinger, W. J., Coriell, S. R., Trivedi, R., Principle and technologies IV, in *Rapid Solidification Processing* (eds. Mehrabian, R., Parrish, P. A.) Baton Rouge: Claitor's Publishing Division, 1988, 13.

13 Aziz, M. J., Model for solute redistribution during rapid solidification, *J. Appl. Phys.*, 1982, 53: 1158.

14 Trivedi, R., Lipton, J., Kurz, W., Effect of growth rate dependent partition coefficient on the dendritic growth in undercooled melts, *Acta Metall.*, 1987, 35: 965.

15 Wu, Y., Piccone, T. J., Shiohara, Y. et al., Dendritic growth of undercooled nickel-tin: Part 3, *Metall. Trans. A*, 1988, 19A: 1109.

16 Willnecker, R., Herlach, D. M., Feuerbacher, B., Evidence of nonequilibrium processes in rapid solidification of undercooled metals, *Phys. Rev. Lett.*, 1989, 62: 2707.

17 Lipton, J., Kurz, W., Trivedi, R., Rapid dendrite growth in undercooled alloys, *Acta Metall.*, 1987, 35: 957.